Nano Today 38 (2021) 101149

Contents lists available at ScienceDirect

Nano Today

journal homepage: www.elsevier.com/locate/nanotoday

Lung-selective 25-hydroxycholesterol nanotherapeutics as a suppressor of COVID-19-associated cytokine storm

Hyelim Kim[a,b,1], Han Sol Lee[a,1], June Hong Ahn[c,1], Kyung Soo Hong[c], Jong Geol Jang[c], Jiseon An[a], Yong-Hyeon Mun[a], So-Yeol Yoo[a], Yoon Jung Choi[a], Mi-Young Yun[d], Gyu Yong Song[a,e], Jinmyoung Joo[f], Dong Hee Na[g,*], Hong Nam Kim[b,h,**], Hee Ho Park[i,j,*], Jae-Young Lee[a,*], Wonhwa Lee[k,*]

[a] College of Pharmacy, Chungnam National University, Daejeon 34134, Republic of Korea
[b] Brain Science Institute, Korea Institute of Science and Technology (KIST), Seoul 02792, Republic of Korea
[c] Division of Pulmonology and Allergy, Department of Internal Medicine, College of Medicine, Yeungnam University and Regional Center for Respiratory Diseases, Yeungnam University Medical Center, Daegu 42415, Republic of Korea
[d] Department of Beauty Science, Kwangju Women's University, Gwangju 62396, Republic of Korea
[e] AREZ Co. Ltd., Daejeon 34134, Republic of Korea
[f] Department of Biomedical Engineering, School of Life Sciences, Ulsan National Institute of Science and Technology (UNIST), Ulsan 44919, Republic of Korea
[g] College of Pharmacy, Chung-Ang University, Seoul 06974, Republic of Korea
[h] Division of Bio-Medical Science and Technology, KIST School, Korea University of Science and Technology, Seoul 02792, Republic of Korea
[i] Department of Biotechnology and Bioengineering, Kangwon National University, Chuncheon, Gangwon-do 24341, Republic of Korea
[j] Interdisciplinary Program in Biohealth-Machinery Convergence Engineering, Kangwon National University, Chuncheon, Gangwon-do 24341, Republic of Korea
[k] Aging Research Center, Korea Research Institute of Bioscience and Biotechnology (KRIBB), Daejeon 34141, Republic of Korea

ARTICLE INFO

Article history:
Received 20 October 2020
Received in revised form 18 March 2021
Accepted 3 April 2021
Available online 8 April 2021

Keywords:
Severe COVID-19
Lung-selective nanohybrids
Sepsis
25-hydroxycholesterol
Didodecyldimethylammonium bromide

ABSTRACT

In response to the coronavirus disease-19 (COVID-19) pandemic caused by severe acute respiratory syndrome coronavirus 2 (SARS-CoV-2), global efforts are focused on the development of new therapeutic interventions. For the treatment of COVID-19, selective lung-localizing strategies hold tremendous potential, as SARS-CoV-2 invades the lung via ACE2 receptors and causes severe pneumonia. Similarly, recent reports have shown the association of COVID-19 with decreased 25-hydroxycholesterol (25-HC) and increased cytokine levels. This mechanism, which involves the activation of inflammatory NF-κB- and SREBP2-mediated inflammasome signaling pathways, is believed to play a crucial role in COVID-19 pathogenesis, inducing acute respiratory distress syndrome (ARDS) and sepsis. To resolve those clinical conditions observed in severe SARS-CoV-2 patients, we report 25-HC and didodecyldimethylammonium bromide (DDAB) nanovesicles (25-HC@DDAB) as a COVID-19 drug candidate for the restoration of intracellular cholesterol level and suppression of cytokine storm. Our data demonstrate that 25-HC@DDAB can selectively accumulate the lung tissues and effectively downregulate NF-κB and SREBP2 signaling pathways in COVID-19 patient-derived PBMCs, reducing inflammatory cytokine levels. Altogether, our findings suggest that 25-HC@DDAB is a promising candidate for the treatment of symptoms associated with severe COVID-19 patients, such as decreased cholesterol level and cytokine storm.

Introduction

Scientists of various disciplines have joined the race to develop therapeutics against the coronavirus disease (COVID-19) pandemic since the outbreak at the end of 2019 [1]. Although most research has focused on eliminating the severe acute respiratory syndrome coronavirus 2 (SARS-CoV-2) itself, it is of vital importance to understand the indispensable role of anti-inflammatory interventions

* Corresponding authors.
** Corresponding author at: Brain Science Institute, Korea Institute of Science and Technology (KIST), Seoul 02792, Republic of Korea.
E-mail addresses: dhna@cau.ac.kr (D.H. Na), hongnam.kim@kist.re.kr (H.N. Kim), hhpark@kangwon.ac.kr (H.H. Park), jaeyoung@cnu.ac.kr (J.-Y. Lee), wonhwalee@kribb.re.kr (W. Lee).
[1] These authors contributed equally: Hyelim Kim, Han Sol Lee, June Hong Ahn.

https://doi.org/10.1016/j.nantod.2021.101149
1748-0132/

in the treatment of COVID-19 [2]. The patients with reduced immunity are vulnerable to SARS-CoV-2 and more prone to develop severe complications, such as cytokine release syndrome (CRS), resulting in excessive and uncontrollable inflammatory responses [3,4]. Recently, it has been suggested that the reduction in blood type I IFNs is one of the hallmarks of severe COVID-19 and thus can be used to screen high-risk patients [5]. The study revealed that impairment of type I IFN activity and its reduced production by SARS-CoV-2 infection trigger exacerbation of inflammation, chemotaxis of monocytes, multiple organ failure, and death [5].

Notably, type I IFN level is closely associated with the regulation of cholesterol 25-hydroxylase (CH25H) expression [6]. CH25H is an enzyme that catalyzes the hydroxylation of cholesterol at carbon position 25 to generate 25-hydroxycholesterol (25-HC) [7]. It is considered that cytokines like type I interferons (IFNs) can provide suppressive effects against the inflammatory responses induced by viral infections. Previously, it was reported that upon infection, the expression of CH25H is increased via induction of type I IFNs through the IFN receptor and the JAK/STAT1 pathway [6]. In addition, it has been reported that 25-HC is a critical inhibitor of sterol regulatory element-binding protein 2 (SREBP2)-mediated cytokine production and apoptosis [8,9]. *Ch25h*-deficient mice demonstrated vulnerability to septic shock, displaying increased neutrophil counts and inflammasome activity via SREBP2 activation [9]. Since 1950s, it has been well established that viral infection induces lowered cholesterol levels [10–18]. In addition, 25-HC possesses broad-spectrum anti-viral activities against coronaviruses, including porcine epidemic diarrhea virus (PEDV) and transmissible gastroenteritis virus (TGEV) [19]. As evidenced by the cases of chloroquine, remdesivir, and lopinavir/ritonavir [20,21], drug repositioning offers a highly efficient and low-cost way to develop therapeutic agents [2]. Given the anti-inflammatory and anti-viral activities, 25-HC was adopted as a drug candidate for the treatment of COVID-19 in our investigation.

More specifically, we hypothesized that the lung-selective delivery of 25-HC could inhibit SARS-CoV-2 replication and suppress excessive inflammatory responses, thereby improving the mortality rate of severe COVID-19 patients. To achieve a high lung deposition of 25-HC, we employed selective organ localization technique [22,23], where 25-HC and didodecyldimethylammonium bromide (DDAB) were fabricated into nanovesicles, namely 25-HC@DDAB. DDAB is a cationic lipid that can serve as not only a 25-HC stabilizing agent by forming liposome-like structures but also a lung-homing moiety by inducing transient erythrocyte agglutination [24–26]. Considering the current situation where no effective therapeutics that can inhibit both viral infection and disease progression towards ARDS or sepsis, our novel nanotherapeutics could hold promise in the fight against COVID-19.

Experimental section

Reagents

Dimethyldioctadecylammonium bromide (DDAB) and 25-hydroxycholesterol (25-HC) were purchased from Sigma-Aldrich Co. (St. Louis, MO, USA). Amine-functionalized Cy5.5 was purchased from BioActs (Incheon, Korea).

Plasma sample

Whole blood was collected from patients admitted at Yeungnam University Medical Center after they were diagnosed with the SARS-CoV-2 infection at the Public Health Center in Daegu, Republic of Korea. Patients with COVID-19 sepsis were defined using criteria provided by the Sepsis Consensus Conference Committee [27]. Pneumonia and septic shock patients were collected from patients admitted at Yeungnam University Medical Center. Healthy volunteers were used as controls. Clinical data were collected for all the patients. Plasma samples were prepared by centrifugation at 2000*g* for 5 min within 12 h after whole blood collection. The human study protocol was approved by the Institutional Review Board of Yeungnam University Hospital at Daegu in Korea (YUH 2020-03-057, 2020-05-031-001). Whole blood was collected from patients after approval for use in the study. Blood sample analysis received at the hospital was conducted in blind. After analysis, it was compared with patient information and then analyzed. MD June Hong Ahn collected patient information and provided blood samples in blinded manner. After receiving the blind samples, Wonhwa Lee, Hong Nam Kim, and Hee Ho Park were in charge of blood analysis and PBMC experiments. Afterwards, all the information was collected and organized, and the patient's personal information were re-analyzed very strictly and accurately by Jinmyoung Joo and Dong Hee Na. Viruses in the blood were observed in COVID-19 patients, and progression toward severe respiratory disease or sepsis was progressed based on the Cohort study of patients. Patients with COVID-19 sepsis were defined using criteria provided by the Sepsis Consensus Conference Committee [27]. Eligible patients met the following criteria: age, over 18 years; and an acute onset medical condition with as at least one of the following criteria: fever (tympanic temperature ≥ 38 °C at the nurse triage), suspected systemic infection, two or more systemic inflammatory response syndrome SIRS criteria, hypotension (systolic blood pressure < 90 mmHg), and/or shock. Healthy volunteers were used as controls. Clinical data were collected for all the patients. COVID-19 patients were categorized depending on the disease severity. “Mild” is defined as patients receiving quarantine treatment in general ward or those with asymptomatic symptoms. “Severe” is defined as patients with ARDS, sepsis, or receiving intensive care in the ICU. It also includes patients treated with oxygen therapy or those that rely on mechanical breathing machines (i.e. ventilators). Similar to previous findings, it was noticeable that most severe patients were elderlies with age over 70 [28].

Quantification of cholesterols in patients blood

The Human 25-Hydroxycholesterol (25-HC) ELISA Kit (MyBioSource, MBS9364825), total cholesterol, HDL-Cholesterol, and LDL-Cholesterol dataset were analyzed using the modular DPE system (Roche Diagnostics, Basel, Switzerland).

Preparation and characterization of lung-localizing 25-HC@DDAB

DDAB and 25-HC were dissolved in methanol and ethanol, respectively. Each solution was blended to be the DDAB/25-HC weight ratio of 2, 4, or 6. The solvent was evaporated for 3 h at 70 °C using a heating block (Eyela MG-2200, Tokyo, Japan). The resulting composite films were resuspended with double-deionized water (DDW) to be the final 25-HC concentration of 1 mg/mL using ultrasonication (VC-750; Sonics & Materials, Inc., Newtown, CT, USA) at an amplitude of 20% with a pulse cycle of 2 s on and 3 s off. Cy5.5-loaded 25-HC@DDAB was prepared using the same method above, except that 70 μg of Cy5.5 was added before the solvent evaporation procedure. The particle size, polydispersity index, and zeta potential of the resulting nanohybrids (NHs) were measured by Zetasizer Ultra (Malvern Panalytical, Malvern, UK) according to the manufacturer's protocol. The morphology of 25-HC@DDAB was observed using transmission electron microscopy (Talos L120C; FEI, Hillsboro, OR, USA) at a cryogenic temperature. The samples (5 μL) were placed onto the surface of carbon-coated copper grids by the plunge-dipping method and vitrified using liquid ethane cooled by liquid nitrogen. The samples were placed onto the surface of carbon-coated copper grids and negatively stained with uranyl acetate. To measure

the drug encapsulation efficiency (EE), the 25-HC concentration of the prepared NH suspension was determined by using a high-performance liquid chromatography (HPLC) system (Agilent 1260 infinity; Agilent Technologies, Palo Alto, CA, USA) equipped with a Kinetex C18 column (4.6 mm × 250 mm, 5 μm; Phenomenex, Torrance, CA, USA). The chromatographic separation was performed in an isocratic elution mode (flow rate: 1.8 mL/min), where the mobile phase consisted of acetonitrile and DDW (80:20, v/v). The detection wavelength for 25-HC was 205 nm. The analytical samples were prepared by disrupting the 25-HC@DDAB with ethanol (40 × volume). The injection volume and lower limit of quantitation (LLOQ) were 20 μL and 1 μg/mL, respectively. The retention time of 25-HC and total run time were 7.8 and 10.0 min, respectively.

Animals and husbandry

Male C57BL/6 mice (6–7-weeks-old, weighing 18–20 g) were purchased from Orient Bio Co. (Sungnam, Korea). Male ICR mice (4-weeks-old, weighing 21–24 g) and female BALB/c nude mice (5-weeks-old, weighing 18–22 g) were purchased from Nara Biotech Co. (Seoul, Korea). The animals were housed 5 per polycarbonate cage under controlled temperature (20–25 °C) and humidity (40–45%) under a 12:12 h light/dark cycle, fed a normal rodent pellet diet, and supplied with water ad libitum. All animals were used after a 12-day acclimatization period and treated in accordance with the Guidelines for the Care and Use of Laboratory Animals issued by Chungnam National University (IRB No.; CNU-01050).

Cecal ligation and puncture (CLP)

For induction of sepsis, male mice were anesthetized with 2% isoflurane (Forane, JW pharmaceutical, South Korea) in oxygen delivered via a small rodent gas anesthesia machine (RC2, Vetequip, Pleasanton, CA), first in a breathing chamber and then via a facemask. They were allowed to breath spontaneously during the procedure. The CLP-induced sepsis model was prepared as previously described [29]. In brief, a 2 cm midline incision was made to expose the cecum and adjoining intestine. The cecum was then tightly ligated with a 3.0-silk suture at 5.0 mm from the cecal tip and punctured once using a 22-gauge needle for induction of high grade sepsis [29]. It was then gently squeezed to extrude a small amount of feces from the perforation site and returned to the peritoneal cavity. The laparotomy site was then sutured with 4.0-silk. In sham control animals, the cecum was exposed but not ligated or punctured and then returned to the abdominal cavity.

In vivo biodistribution of 25-HC@DDAB

Male ICR mice were injected with free Cy5.5 or Cy5.5-loaded 25-HC@DDAB via tail vein at a Cy5.5 dose of 35 μg/kg. Free Cy5.5 injection solution was prepared by diluting an aliquot (7 μL) of Cy5.5 stock solution (1 mg/mL, dissolved in DMSO) with normal saline (993 μL) by vortex-mixing. At each time point (3, 6, 9, 12, 24, and 48 h post-injection), three biologically independent animals were sacrificed and their organs (liver, kidney, spleen, heart, and lung) were dissected for *ex vivo* imaging. The biodistribution of free Cy5.5 or Cy5.5-loaded 25-HC@DDAB was monitored by measuring fluoresce intensity of each organ using VISQUE® InVivo Smart (Vieworks, Anyang, Korea). As control carriers, egg phosphatidylcholine (EPC; Lipoid E100; Lipoid AG, Ludwigshafen, Germany)-blended NHs, including Cy5.5-loaded 25-HC@EPC and Cy5.5-loaded 25-HC@DDAB/EPC, were fabricated using the aforementioned method (see *Preparation and characterization of lung-localizing 25-HC@DDAB)*, except that the feed ratios of DDAB/EPC/25-HC were set at 0/4/1 and 2/2/1, respectively. These control carriers were also evaluated using the same experimental design above. At 6 h post-injection, the animals were euthanized, and their major organs were eviscerated for imaging. The radiant efficiency value of each organ was compared with that of 25-HC@DDAB. Cy5.5-loaded 25-HC@DDAB was also administered to the male ICR mice intravenously 12 h after CLP operation at the same Cy5.5 dose. The mice were euthanized at 3, 6, and 12 h post-injection, and the *ex vivo* imaging was performed on the major organs according to the same protocol above. For in vivo imaging, CLP-operated BALB/c nude mice were administered with Cy5.5-loaded 25-HC@DDAB at a Cy5.5 dose of 35 μg/kg, and the whole-body scan was carried out at 30, 60, 90, 120, 180, 240, and 360 min post-injection. The radiant efficiency of the thorax region was measured using CleVue™ software (Vieworks).

PBMC isolation and culture

Samples from healthy, SARS-CoV-2 pneumonia patients, or discharged patients were obtained from Yeungnam University Medical Center. The relevant local Institutional Review Boards and Ethics Committees approved the study. Heparinized blood samples were used fresh within 4 h, and peripheral blood mononuclear cells (PBMCs) were separated from blood using Ficoll–Hypaquek or NycoPrepk according to the manufacturer's recommendations. Following this, more refined PBMCs were obtained via MACSprep™ PBMC Isolation Kit and cultured in RPMI-1640 with 1 mM Sodium pyruvate, 2 mM L-glutamine, 4.5 mg/L glucose, 10 mM HEPES and 2 mg/L sodium bicarbonate.

Western blotting

Ch25h were detected by immunoblotting, in separated PBMCs from mild COVID-19 or severe COVID-19. After sodium dodecyl sulfate polyacrylamide gel electrophoresis, we performed an immunoblotting assay with monoclonal mouse anti-Ch25h antibodies (CH25H monoclonal antibody (M01), clone 1G8, H00009023-M01, Abnova).

Inflammatory cytokines IL-1β, and TNF-α ELISAs

Serum levels of inflammatory cytokines IL-1β, and TNF-α were determined in SARS-CoV-2-infected patients using human ELISA kits (Quantikine ELISA, R&D Systems, Minneapolis, MN, USA) according to the manufacturer's instructions. PBMCs isolated from patient blood were treated with 0.5 or 1.0 μM 25-HC or 25-HC@DDAB for 12 h. The results were expressed as pg/mL.

WST-1 cell proliferation assay

10 μL per well of WST-1 reagent were added in purified PBMC, HUVECs, or MRC-5 (human fetal lung fibroblast cell line) and incubated at 37 °C with 5% CO_2. At indicated time points, measurements of absorbance were taken at 480 nm and 600 nm (background) on Tecan Spark microplate reader.

Cytokines profiling

PBMCs isolated from patient blood were treated with 0.5 or 1.0 μM 25-HC or 25-HC@DDAB for 12 h. Plasma pools of patients with normal or severe COVID-19 patients were processed as indicated in the Human XL Cytokine Array Kit (R&D Systems). Developed films were scanned, the obtained images were analyzed using ImageJ version 1.43.

Real-time PCR

PBMCs isolated from patient blood were treated with 0.5 or 1.0 μM 25-HC or 25-HC@DDAB for 12 h. To generate cDNA from PBMCs, SN50/Fatostatin A treated PBMCs, or SN50/Fatostatin A

administrated septic mouse lung tissue samples, 1 μg of total RNA was reverse transcribed with random hexamers using expand reverse transcription polymerase (Roche). Real-time PCR was performed using the LightCycler FastStart DNA Master SYBR Green I from Roche Diagnostics GmbH according to the manufacturer's protocol. The following LightCycler conditions were used: Initial denaturation at 95 °C for 10 min, followed by 45 cycles with denaturation at 95 °C for 10 min, annealing at 60 °C for 5 min, and elongation at 72 °C for 15 min. Quantities of specific mRNA in the sample were measured according to the corresponding gene-specific standard curves.

Gene symbol	Forward primer	Reverse primer
SREBF2	CCTTCCTGTGCCTCTCCTTTA	AGGCATCATCCAGTCAAACCA
IL1B	TACCTGTCCTGCGTGTTGAAA	CTGCTTGAGAGGTGCTGATGT
TNF	TGGCGTGGAGCTGAGAGATAA	TTGATGGCAGAGAGGAGGTTGA
NLRP3	TGCCGGGGCCTCTTTTCAGT	CCACAGCGCCCCAACCACAA
NOX	AACGAATTGTACGTGGGCAGA	GAGGGTTTCCAGCAAACTGAG
MCP-1	CGCTCAGCCAGATGCAATCAATGC	GGTTTGCTTGTCCAGGTGGTCCA
Srebf2	TGTGGCTGGTAAATGGTGTGA	AGCACGGATAAGCAGGTTTGT
Nox2	ACTCCTTGGAGCACTGG	GTTCCTGTCCAGTTGTCTTCG
Nlrp3	TCGCCCAAGGAGGAAGAAGAA	TGAGAAGAGACCACGGCAGAA
Il-1β	GGTGTGTGACGTTCCCATTAG	TCGTTGCTTGGTTCTCCTTGT
Icam-1	GCTACCATCACCGTGTATTCG	TAGCCAGCACCGTGAATGTG
Mcp-1	TTAAAAACCTGGATCGGAACCAA	GCATTAGCTTCAGATTTACGGGT
β-actin	CATGTACGTTGCTATCCAGGC	CTCCTTAATGTCACGCACGAT

Isolation of endothelial cell from mouse

The endothelial cells were isolated according to the manufacturer's (Dynal Biotec, Lake Success, NY) instructions, using Dynabeads coupled to anti-CD31 antibody and the Dynal Magnetic holder. Briefly, for endothelial cell isolation, four to six mice (6–10 weeks old) were anesthetized, followed by exposure of the peritoneal cavity. Excised lungs and hearts put into RPMI media and remove other tissues from heart and lungs, and then rinse once in PBS. The lung and hearts incubate with 1.0 mg/mL of collagenase A in a 50 mL tube for 1 h, rocking at 37 °C. Every 5 min during this incubation, the tube was gently agitated for a few seconds, and then transfer the suspension into a new 50 mL tube by passing it through the 70 μm tissue sieve (BD Falcon). The filtered cell suspension was centrifuged for 10 min at 1000 rpm. After removal of the supernatant, the cell pellet was washed once with cold PBS in a new 15-mL tube. To prepare the Dynabead-coupled anti-mouse CD31 antibody, Dynabeads (60 μL) were washed with MACS buffer (PBS, 0.5% BSA, 2 mM EDTA) on a magnetic holder (Invitrogen). The Dynabeads were resuspended with MACS buffer (600 μL), anti-mouse CD31 (5 μg of per 10 μL of beads) was added, and the mixture was incubated for 12 h at 4 °C. Cells were incubated with Dynabead-coupled anti-mouse CD31 antibody for 10 min at room temperature and then placed in a magnetic holder. Cell suspension was slowly added to a 15 mL tube by placing the pipette on the wall of the tube. After incubation for 5 min, PBS was carefully removed by aspiration. The Dynabead-coupled anti-mouse CD31 antibodies were washed three times in cold PBS, the pellet was resuspended in EBM-2 growth medium, and then harvested and lysed in RIPA buffer containing protease inhibitor cocktail (Roche) on ice.

Cholesterol staining by filipin

Mouse lung endothelial cells were seeded in a Nunc Lab-Tek II 8-Chamber Slide and treated with compounds for indicated time points. Cells were fixed with 4% paraformaldehyde for 1 h at room temperature and then permeabilized with 0.5% Triton X-100 (for protein immunostaining) for 10 min prior to blocking in a blocking buffer (3% bovine serum albumin (BSA) in PBS containing 0.1% Tween-20) for 12 h. Cells were incubated with Filipin staining dye in the blocking buffer overnight at 4 °C. Cells were washed with PBS, mounted with Immu-mount, and were visualized by fluorescence microscopy at a 200× magnification (Leica microsystem, Germany). The 25-HC@DDAB was treated at a concentration of 0.1, 1, and 10 μM for 24 h.

Quantification of 25-HC concentration in lung microsomes of septic mice

ICR mice (6-week-old) were administered with 1.0 μM 25-HC@DDAB intravenously 12 h after the CLP operation. At 6 h post-injection, the mice were euthanized and the lung was dissected. The lung tissue homogenate (10%, w/v) was prepared using T25 Ultra-Turrax® (IKA-Werke GmbH & Co. KG, Staufen, Germany), wherein the lung was homogenized with PBS at 15,000 rpm for 1 min on ice. To isolate microsomes, the lung homogenate was first centrifuged at 20,000*g* for 15 min at 4 °C using Beckman XL-80 ultracentrifuge (Beckman Instruments, Inc., Fullerton, CA, USA). Subsequently, the supernatant was collected and centrifuged at 100,000*g* for 60 min at 4 °C. The pellet (microsomes) was collected and resuspended using the test buffer of 25-HC ELISA kit (MyBioSource, MBS7254215). The quantification of 25-HC concentration in the microsomal suspension was carried out according to the manufacturer's protocol.

Cytotoxicity test

Mouse lung endothelial cells were treated with various concentrations of 25-HC@DDAB for 24 h and stained using LIVE/DEAD™ Fixable Far Red Dead Cell Stain Kit (L34973, Invitrogen™). Cells were then washed twice with PBS. Stained cells were resuspended in 1 mL of PBS, and the fluorescence was quantified using a FACScan flow cytometer (BD).

Hematoxylin and eosin staining

Male C57BL/6 mice underwent CLP and were administered 25-HC, and 25-HC@DDAB (1 μM) intravenously at 6 h after CLP (n = 5). Mice were euthanized 96 h after CLP. To analyze the phenotypic change of lung in mice, lung samples were removed from each mouse, washed three times in PBS (pH 7.4) to remove remaining blood, fixed in 4% formaldehyde solution (Junsei, Tokyo, Japan) in PBS, pH 7.4 for 20 h at 4 °C. After fixation, the samples were dehydrated through ethanol series, embedded in paraffin, sectioned into 4-μm sections, and placed on a slide. The slides were deparaffinized in a 60 °C oven, rehydrated, and stained with hematoxylin (Sigma). To remove over-staining, the slides were quick dipped three times in 0.3% acid alcohol, and counterstained with eosin (Sigma). They are then washed in ethanol series and xylene, and then cover slipped. Light microscopic analysis of lung specimens was performed by blinded observation to evaluate pulmonary architecture, tissue edema, and infiltration of the inflammatory cells.

Clinical chemistry and cytokine level in septic mice plasma

Fresh serum was used for assaying aspartate transaminase (AST), alanine transaminase (ALT), blood urea nitrogen (BUN), creatinine, and LDH using biochemical kits (Mybiosource). To determine the concentrations of IL-1β, IL-6, IL-10, monocyte chemoattractant protein-1 (MCP-1), and TNF-α commercially available ELISA kits were used according to the manufacturer's protocol (R&D Systems). Values were measured using an ELISA plate reader (Tecan, Austria GmbH, Austria).

In vivo permeability and leukocyte/neutrophil migration assays

CLP-operated mice were injected with 25HC or 25-HC@DDAB intravenously. After 6 h, 1% Evans blue dye solution in normal saline was injected intravenously into each mouse. Thirty minutes later, the mice were killed, and the peritoneal exudates were collected after being washed with normal saline (5 mL) and centrifuged at 200 × *g* for 10 min. The absorbance of the supernatant was read at 650 nm. The vascular permeability was expressed in terms of dye (μg/mouse), which leaked into the peritoneal cavity according to a standard curve of Evans blue dye.

For assessment of leukocyte/neutrophil migration, CLP operated mice were treated with 25-HC@DDAB (1 μM) after CLP surgery 6 h. The mice were then sacrificed and the bronchoalveolar lavage (BAL) were washed with 0.8 mL of normal saline [30]. BAL fluid (200 μL) was counted by auto hematology analyzer (Mindray, BC 5000 Vet). The results were expressed as leukocyte/neutrophil × 10^5 per BAL fluid.

Expression of ICAMs

The expression of intercellular adhesion molecule-1 (ICAM-1) on lung tissues was determined by a direct ELISA. The lysed lung tissues were coated onto Nunc-Immuno™ MicroWell™ 96 well plates and incubated overnight at 4 °C. After washing, anti-mouse monoclonal ICAM-1 antibodies (Millipore Corporation, Billerica, MA, 1:50 each) were added. After 1 h (37 °C, 5% CO_2), the cells were washed three times and then 1:2000 peroxidase-conjugated anti-mouse IgG antibody (100 μL; Sigma, Saint Louis, MO) was added for 1 h. The cells were washed again three times and developed using the *o*-phenylenediamine substrate (Sigma, Saint Louis, MO). Colorimetric analysis was performed by measuring absorbance at 490 nm. All measurements were performed in triplicate wells.

Cytokine levels in the plasma of septic mice

Fresh serum was used for analysis of AST, ALT, BUN, creatinine, and LDH levels using biochemical kits (MyBioSource). Values were measured using an ELISA plate reader (Tecan, Austria GmbH, Austria).

SREBP-2 transcriptional activity assays

The transcriptional activities of SREBP-2 were determined by the ELISA method using kits from Abcam (ab133111, Abcam) following manufacturer's protocol. Briefly, nuclear homogenate equivalent to 30 μg of the protein content was added to each of the wells of the 96-well plate containing the double-stranded DNA sequence harboring the consensus SREBP-binding sequence (sterol regulatory element, SRE) coated onto the wells. The nuclear extract was allowed to hybridize with the coated double-stranded DNA sequence harboring the consensus SRE (sterol regulatory element) in the plate overnight at 4 °C. The activated SREBP transcription factor complex was detected by addition of a specific primary antibody directed against SREBP-2 and a secondary antibody conjugated to HRP added to provide a sensitive colorimetric readout at 450 nm.

NF-κB transcriptional activity assays

Preparation of nuclear extracts and TransAM assays were performed as previously described [31]. The activity of individual NF-κB subunits was determined using an ELISA-based NF-κB Family Transcription Factor Assay Kit (43296; Active Motif, Carlsbad, CA, USA). Briefly, nuclear extracts (2 μg) were incubated in a 96-well plate, which was coated with NF-κB consensus oligonucleotides. The captured complexes were incubated with specific NF-κB primary Abs and subsequently detected using HRP-conjugated secondary Abs included with the kit. Finally, the optical density (OD) at 450 nm was measured using a Tecan Spark microplate reader (Tecan, Austria GmbH, Austria).

Statistical analysis

All the in vitro and in vivo data were analyzed via two-tailed unpaired *t*-test using the Graphpad prism 7 software, the prepared sample sizes were n ≥ 3, and the statistical significance was set at $P < 0.05$. A more detailed information for each experiment is provided in the figure legend. All data normalization processes were carried out according to the manufacturer's protocol. Data transformation and evaluation of outliers were not used in our study.

Results

Decreased 25-HC, LDL, HDL, and total cholesterol in severe COVID-19 patients

According to the analysis of COVID-19 patients' plasma, we found that the levels of blood cholesterol, including 25-HC, low-density lipoprotein (LDL) cholesterol, high-density lipoprotein (HDL) cholesterol, and total cholesterol, were significantly reduced in severe cases of COVID-19 patients compared to mild cases (Fig. S1a). Similar to previous findings, it was noticeable that most severe patients were elderlies with age over 70 [28]. Among them, the level of 25-HC decreased more than six-fold from 17.5 ± 10.5 μg/mL to 2.8 ± 4.9 μg/mL. Noteworthy is that patients with a low 25-HC level exhibited more severe signs of lung inflammation, as can be seen in the chest computed tomography (CT) images (Fig. S1b).

Preparation and characterization of 25-HC@DDAB

However, due to the poor water solubility (≈224 ng/mL), the intravenous administration of 25-HC should be preceded by an appropriate solubilization procedure. Inspired by a conventional liposome structure composed of vesicle-forming amphiphilic lipids and membrane-stabilizing cholesterols, we successfully prepared 25-HC@DDAB via the film-hydration method, which displayed vesicle-like morphology (Fig. 1a and b). Dynamic light scattering analysis revealed that nanohybrids (NHs) with DDAB/25-HC weight ratio of 4 showed an optimal average diameter of 126.5 ± 2.3 nm (polydispersity index [PDI] of 0.26 ± 0.01) and positively-charged zeta potential of 93.26 ± 3.84 mV. The NHs with DDAB/25-HC weight ratio of 2 or 6 were excluded from further investigations due to the larger particle size (179.3 ± 8.6 nm) or broader size distribution (PDI of 0.72 ± 0.10), respectively, compared to those with the weight ratio of 4. The encapsulation efficiency of 25-HC was determined to be 101.7 ± 1.3% by using high-performance liquid chromatography analysis. Cy5.5 was loaded to the nanohybrids as a fluorescent probe, of which mean diameter was 204.2 ± 4.1 nm (Fig. 1c and d). It is worth noting that the intravenously administered NHs exhibited preferential accumulation to the lung with high efficiency compared to the other organs (Fig. 1e and f). Even 48 h after the administration, the average radiant efficiency of the lung in the NH-treated group was 2.6-fold higher than that in the free Cy5.5-treated group ($p < 0.05$) (Fig. 1g). This lung localization of NHs can be explained by the transient aggregation with red blood cells (RBCs) via electrostatic interactions [22,23]. More specifically, the NHs administered via peripheral vein first encounter RBCs. Due to the electrostatic attractions between NHs (positively-charged) and RBCs (negatively-charged), transient aggregates can be generated in the blood stream, which are then perfused into the pulmonary circulation. The transient aggregates with large particle size can be retained in the pulmonary capillary, increasing the chances of lung retention of NHs. Notably, negatively-charged or less positively-charged

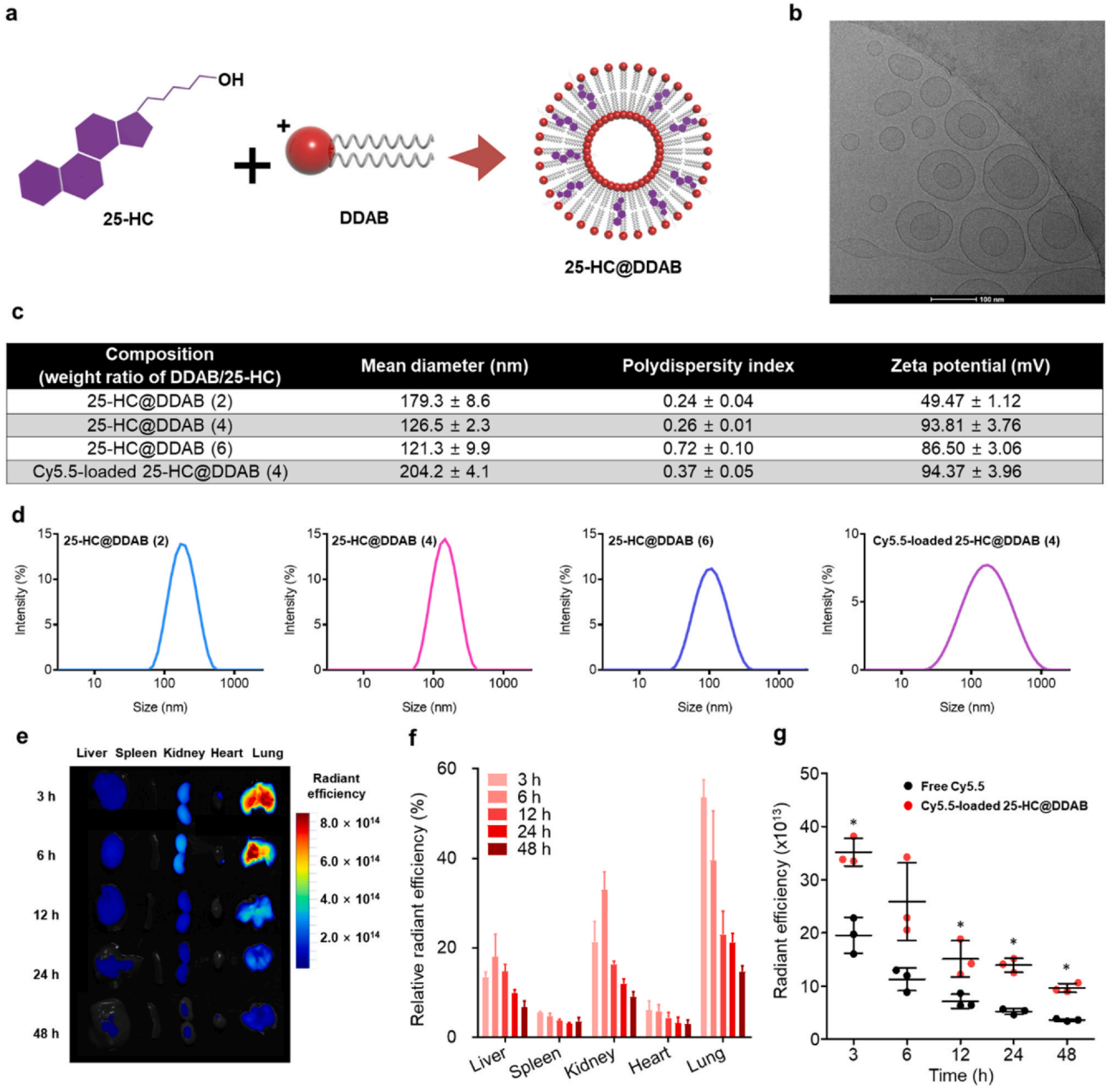

Composition (weight ratio of DDAB/25-HC)	Mean diameter (nm)	Polydispersity index	Zeta potential (mV)
25-HC@DDAB (2)	179.3 ± 8.6	0.24 ± 0.04	49.47 ± 1.12
25-HC@DDAB (4)	126.5 ± 2.3	0.26 ± 0.01	93.81 ± 3.76
25-HC@DDAB (6)	121.3 ± 9.9	0.72 ± 0.10	86.50 ± 3.06
Cy5.5-loaded 25-HC@DDAB (4)	204.2 ± 4.1	0.37 ± 0.05	94.37 ± 3.96

Fig. 1. Preparation and evaluation of 25-HC@DDAB nanohybrids (NHs) for lung tissue localization. (a) Schematic illustration of 25-Hydroxycholesterol@Didodecyldimethylammonium bromide (25-HC@DDAB) NHs. (b) Transmission electron microscopy (TEM) image of 25-HC@DDAB. The length of scale bar is 100 nm. (c) Characterization of 25-HC@DDAB NHs. Intensity averaged hydrodynamic diameters with polydispersity index and zeta potential values are presented. (d) Size distribution diagrams of 25-HC@DDAB NHs are displayed. (e) *Ex vivo* imaging of dissected organs after the intravenous administration of Cy5.5-loaded 25-HC@DDAB. Representative images from each group are shown (n = 5). (f) Relative radiant efficiency of each organ, where the sum of radiant efficiency values of liver, spleen, kidney, heart, and lung at 3 h is set as 100%. (g) Average radiant efficiency in the lung of Cy5.5-loaded NH-treated group was compared with that of free Cy5.5-treated group according to the elapsed time after administration. Statistical analysis was performed using a two-tailed unpaired *t*-test. Data are presented as mean ± standard deviation. *P < 0.05.

control NHs displayed a significantly compromised lung distribution compared to 25-HC@DDAB, which indicates that the enhanced lung disposition of the developed NHs can be attributed to their positively-charged zeta potential (Fig. S2). The mouse lung tissue lysate also showed a higher level of 25-HC upon the delivery of 25-HC@DDAB than 25-HC alone, supporting the enhanced lung delivery efficiency of the developed NHs (Fig. S2). The improved lung distribution suggests that 25-HC@DDAB can be an efficient tool for treating respiratory diseases. Although most 25-HC@DDAB was localized in the lung tissue after intravenous injection, the agents could still remain in blood circulation, causing undesirable vascular toxicity. Thus, we evaluated cytotoxic effect of the 25-HC DDAB in the in vitro-cultured mouse lung endothelial cells (Fig. S3a). The mouse lung endothelial cells showed no significant cytotoxic effect (Fig. S3b). We also evaluated cytotoxic effect of the 25-HC DDAB in the in vitro-cultured human lung endothelial cell (HUVEC) and human fetal lung fibroblast cell line (MRC5). The human lung cells showed no significant cytotoxic effect (Fig. S4). Moreover, intravenous administration 25-HC@DDAB demonstrated no hematotoxicity and organ damage (Fig. S5). The filipin staining, which was used for the visualization of intracellular cholesterol level, confirmed the high level of intracellular cholesterol in isolated mouse lung endothelial cells from the 25-HC@DDAB-administered mouse (Fig. S3). This result can be attributed in part to the positively-charged surface of NHs that allows enhanced cellular uptake via interaction with the negatively-charged cell surface.

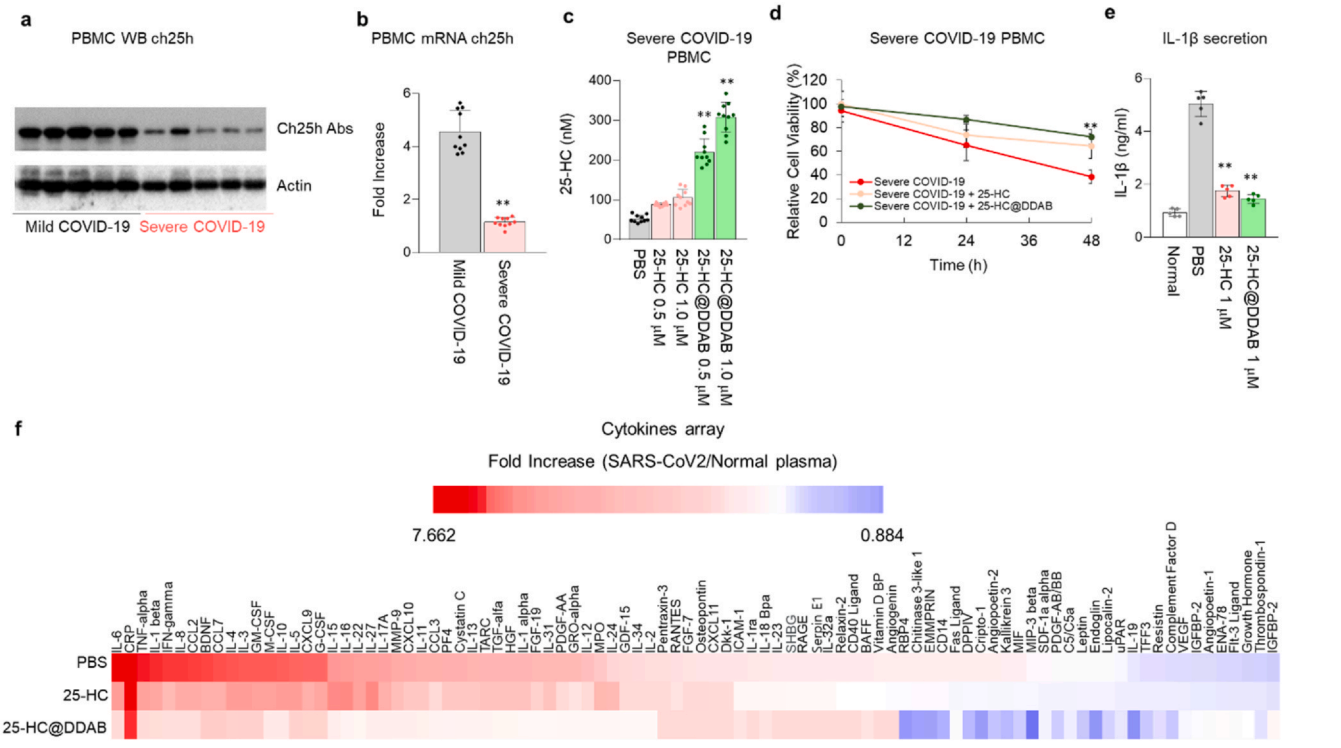

Fig. 2. 25-HC@DDAB suppressed cytokine storm in the PBMCs of severe COVID-19 patients. (a) Western blot analysis of Ch25h level in PBMCs of mild and severe COVID-19 patients (n = 5/each group). (b) qRT-PCR analysis of ch25h mRNA level (n = 10/each group). (c) Level of 25-HC upon the treatment of 25-HC and 25-HC@DDAB with 0.5 μM and 1.0 μM concentrations (n = 10/each group). (d) Effect of 25-HC and 25-HC@DDAB in the rescue of survival rate of PBMCs derived from severe COVID-19 patients (n = 10/each group). (e) Effect of 25-HC and 25-HC@DDAB in the suppression of IL-1β production quantified by ELISA (n = 5/each group). (f) Effect of 25-HC and 25-HC@DDAB in the suppression of cytokine storm as confirmed by cytokine array analysis (n = 3/each group). For the assay, 2×10^6/well of cells per group was treated with 1 μM 25-HC and 25-HC@DDAB in RPMI medium without FBS for 12 h. Statistical analysis was performed using a two-tailed unpaired *t*-test. **P < 0.01.

Treatment of 25-HC@DDAB ameliorates cytokine storm on PBMC of severe COVID-19 patients

The peripheral blood mononuclear cells (PBMCs) were isolated from COVID-19 patients' blood and analyzed with the western blot to confirm the level of CH25H. Indeed, the enzyme level was lower in the PBMCs derived from severe COVID-19 patients than those from mild COVID-19 patients (Fig. 2a). The mRNA expression of *CH25H* was also downregulated in the PBMCs isolated from severe COVID-19 patients (Fig. 2b). Interestingly, the treatment of 25-HC@DDAB significantly increased the 25-HC level in PBMCs of severe COVID-19 patients in a dose-dependent manner (Fig. 2c). As a result of 25-HC@DDAB treatment, the cell viability of PBMCs derived from severe COVID-19 patients was rescued (Fig. 2d). Notably, it was demonstrated that the 25-HC@DDAB could inhibit the cytokine storm. As confirmed by enzyme-linked immunosorbent assay (ELISA) (Fig. 2e) and cytokine array (Fig. 2f), the 25-HC@DDAB inhibited the excessive production of IL-1β, a well-known cytokine involved in cytokine storm. Considering that the vascular and lung damages are attributed to cytokine storm, the 25-HC@DDAB showed promising ability as a mediator of the cytokine storm. We utilized two analytical techniques to evaluate the efficacy of 25-HC@DDAB for the suppression of cytokine storm; enzyme-linked immunosorbent assay (ELISA) and cytokine array. Although the uptake efficiency of 25-HC@DDAB was higher than that of 25-HC, the reduced level of IL-1β was similar, presumably due to the sufficient uptake of 25-HC during the 12 h treatment period. The expression level of IL-6 was demonstrated in Fig. 2f, in which the treatment of 25-HC@DDAB reduced the expression level of IL-6. We believe that, at least in the in vitro assay, the 25-HC@DDAB can suppress the cytokine storm in the COVID-19 patient-derived PBMCs. Recently, it was reported that NLRP3 inflammasome is activated via cholesterol master transcription factor, SREBP2 [32]. It may be possible that sterol depletion promotes NLPR3 inflammasome activation in the lungs and leads to intracellular delivery of 25-HC. Additionally, the 25-HC@DDAB reduced the activation level of SREBP2, which is known to activate inflammation and TNF-α overproduction (Figs. S6 and S7). The mRNA levels related to inflammation (IL-1β and TNF-α), reactive oxygen species formation (NOX2), and activation of NF-κB signaling (NRLP3) that regulates inflammation were downregulated in the PBMCs derived from severe COVID-19 patients with the benefit of 25-HC@DDAB (Fig. S8). The monocyte chemoattractant protein 1 (MCP1), which regulates the chemokine related to vascular inflammatory responses, and SREBP2 were also downregulated (Fig. S8). These results consistently suggest that 25-HC@DDAB could ameliorate the cytokine storm and inflammasome-mediated apoptosis by inhibiting SREBP2 activation.

25. -HC@DDAB increase survival rate of septic mouse model

To demonstrate the capability of 25-HC@DDAB as a therapeutic agent for treating respiratory infectious diseases, a cecal ligation and puncture (CLP) animal model was utilized. Although the CLP-treated mice showed lethal outcomes, the 25-HC rescued the survival rate to 30% and the 25-HC@DDAB to 50% (Fig. 3a). The histological analysis of lungs from sacrificed mice showed reduced damages to the blood vessel and lung tissue in the 25-HC@DDAB treated case (Fig. 3b). The plasma analysis of sacrificed mice showed a lower level of 25-HC in the blood in the case of 25-HC@DDAB, implying the higher uptake by tissue cells (Fig. 3c). The indicators related to inflammation were rescued in the 25-HC@DDAB treated groups, such as permeability, intercellular adhesion molecules 1 (ICAM-1) expression in lung tissue, leukocyte and neutrophil migration in bronchoalveolar lavage (BAL), and SREBP2 activity in lung tissue (Fig. 3c). The markers for sepsis including C-reactive protein (CRP), lactate dehydrogenase (LDH), alanine aminotransferase (ALT), aminotransferase (AST),

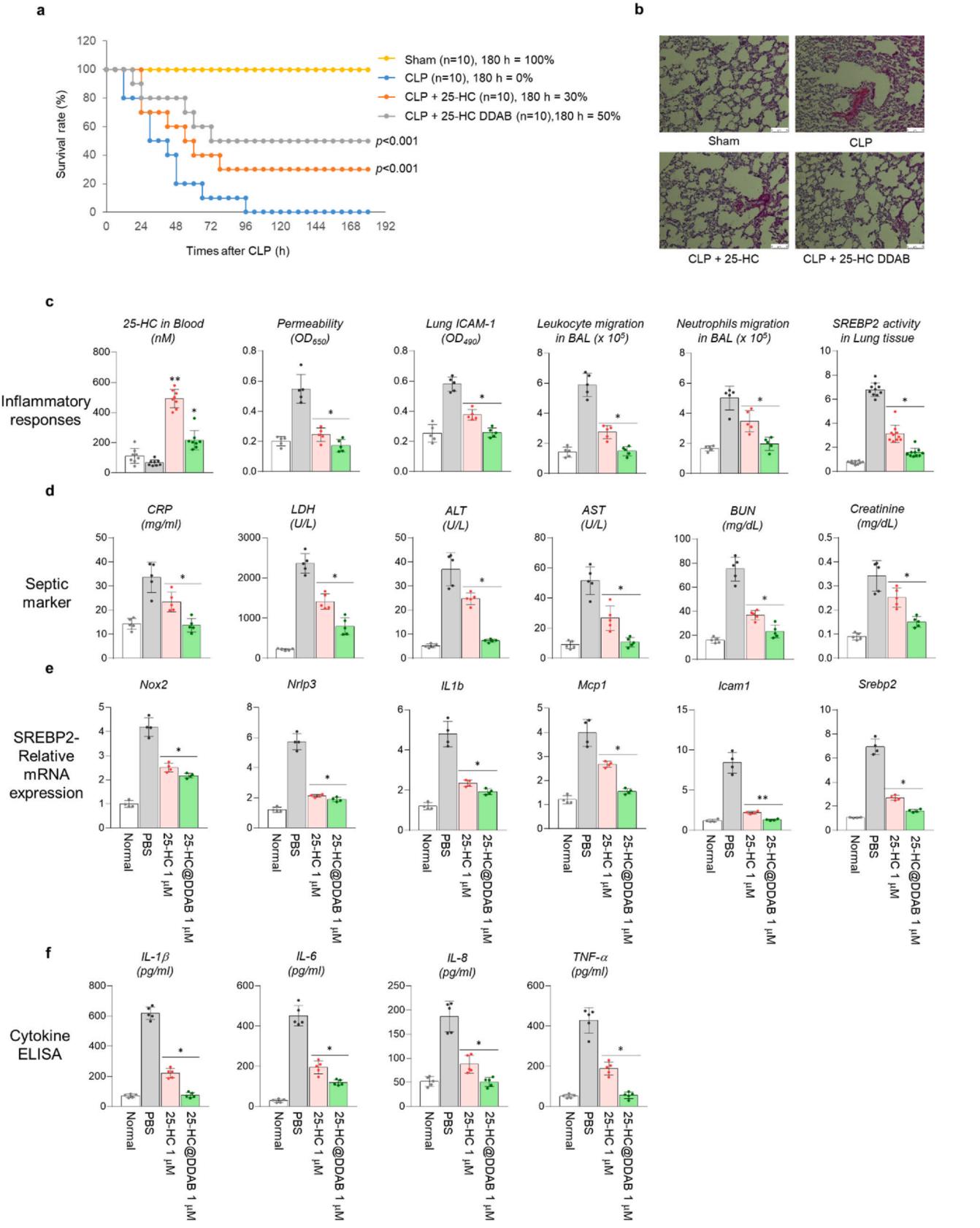

(caption on next page)

Fig. 3. Effect of 25-HC and 25-HC@DDAB in the rescued survival rate of septic mice model. (a) Time-course survival rate of the cecal ligation and puncture (CLP) mice model after the treatment of 25-HC and 25-HC@DDAB (n = 10/each group). (b) Histological analysis of lung tissue from CLP mice models. The administration of 25-HC@DDAB reduced the blood vessel rupture and lung tissue damage. Representative images from each group are shown (n = 5). Scale bar, 100 μm. (c) Changes of inflammation-related signatures in mice models after the administration of 25-HC and 25-HC@DDAB after the CLP treatment. The in vivo signatures includes serum 25-HC level (n = 10), vascular permeability (n = 5), ICAM-1 (n = 5) level in lung tissue, leukocyte (n = 5) and neutrophil migration (n = 5) in bronchoalveolar lavage (BAL), and SREBP2 activity (n = 10) in lung tissue. (d) Changes of septic markers in the blood of 25-HC and 25-HC@DDAB treated CLP mouse models. The markers include CRP, LDH, ALT, AST, BUN, and creatinine (n = 5). (e) Changes of SREBP2-related mRNA expression after the treatment of 25-HC and 25-HC@DDAB. The mRNAs related to SREBP2 are Nox2, Nrlp3, IL1b, Mcp1, Icam1, and Srebp2 (n = 5). (f) Changes of cytokine levels after the treatment of 25-HC and 25-HC@DDAB in CLP mouse models. The cytokines include IL-1β, IL-6, IL-8, and TNF-α (n = 5). Statistical analysis was performed using a two-tailed unpaired *t*-test. $^{*}P < 0.05$, $^{**}P < 0.01$.

blood urea nitrogen (BUN), and creatinine were also reduced in the 25-HC@DDAB treated mouse plasma (Fig. 3d). The absolute neutrophil count (ANC) was decreased, and absolute leukocyte count (ALC) was increased in the 25-HC@DDAB treated group (Fig. S8). Moreover, the SREBP2-related mRNA expression, including *Nox2*, *Nrlp3*, *Il1b*, *Mcp1*, *Icam1*, and *Srebp2,* was reduced upon the treatment of 25-HC@DDAB in mouse models (Fig. 3e). As expected, the serum cytokine levels such as IL-1β, IL-6, IL-8, and TNF-α were decreased in the 25-HC@DDAB treated group, confirming the capability of 25-HC@DDAB as a cytokine storm inhibitor (Fig. 3f).

Discussion

Since the outbreak of COVID-19 infectious disease, a few studies have reported reduced levels of serum cholesterol in COVID-19 patients [33]. The reduced serum cholesterol level is associated with poor clinical outcomes, such as the development of myocardial infarction. Because the low serum cholesterol level is also related to vulnerability to viral infection, treatment strategies via supplementation of exogenous cholesterol, such as 25-HC, have been utilized in coronavirus infections [19]. This previous report encouraged us to evaluate the therapeutic benefits of 25-HC in COVID-19 treatment. For efficient delivery of 25-HC to the lung tissue, we adopted DDAB, a cationic surfactant that possesses amphiphilic structure. Due to the polar head (ammonium) and non-polar tails (didodecyl chains), DDAB formed cationic liposome-like structures with 25-HC. Interestingly, the resulting NHs exhibited highly-enhanced lung localization (Figs. 1e, f and S2), as well as improved cellular uptake of 25-HC in isolated mouse lung endothelial cells (Fig. S3) compared to 25-HC alone. The enhanced intracellular transport with the aid of DDAB increased the 25-HC concentration in the endoplasmic reticulum (Fig. S2h) and promoted the efficacy of 25-HC-mediated cytokine suppression and downregulation of inflammation-related signaling. Notably, intracellular invasion of SARS-CoV-2 virus by recognizing the ACE2 receptors in the lung leads to COVID-19 infection, resulting in significant lung tissue damage and inflammation[34,35] Therefore, selective lung localizing capability of 25-HC@DDAB could be a significant finding towards the development of therapeutics for virus-mediated infectious respiratory diseases.

The major causes of death from bacterial or viral infections are mostly ARDS and sepsis [36]. It is well-known that deadly viruses or bacteria can cause cytokine storms in the blood, causing severe vascular inflammation that leads to multiple organ failure (MOF) [37,38]. The mortality rate at the onset of sepsis is very high [39], where no sign of improvement even after the clearance of the infectious agents often leads to poor prognosis [40]. Thus, the development of drug candidates that can suppress cytokine storms and prevent MOF is vital to the establishment of an efficient therapeutic regimen for infectious diseases like COVID-19 [41,42]. According to the experiment conducted in sepsis animal model, the 25-HC@DDAB was proven to be effective in sepsis. Upon the septic condition, the administration of 25-HC@DDAB exhibited its efficacy within 48 h and increased the survival rate by 50% (Fig. 3a). According to the ELISA and RT-PCR analyses, the administered 25-HC@DDAB suppressed inflammation, septic marker expression, and cytokine overproduction (Figs. 3c–e and S7–S9). Especially, the 25-HC regulated the SREBP2 signaling, which is known as a critical mediator of inflammation and downstream signaling of NF-κB [43,44]. The inhibition of SREBP2 could effectively suppress the cytokine storm.

The correlation of the dysregulated cholesterol level and severity of COVID-19 infectious disease is an important issue. 25-HC is produced as a result of cholesterol oxidation, and this oxidation is regulated by the enzyme cholesterol-25-hydroxylase. Recent studies found that the increased level of 25-HC in the severe COVID-19 patients' sera [45], and the exogenous treatment in the SARS-CoV-2-infected cells and hACE2 mice models decreased the viral load. In terms of the mechanism, the 25-HC blocks the membrane fusion between the viral and cell membranes, acting as a SARS-CoV-2 inhibitor [45,46]. In regards to biosafety, it was shown that administration of 25-HC at 1000 mg/kg did not cause any adverse effects in mice models [45]. According to their recent reports, the serum level of 25-HC was increased while other cholesterol levels were decreased. These results demonstrate that the administered 25-HC does not compensate for the reduced 25-HC level, but rather regulates the viral load.

Recently, the World Health Organization (WHO) welcomed the dexamethasone being a promising candidate for severe COVID-19 treatment. Its initial clinical trial demonstrated that regulation of inflammation is a key factor for the treatment of COVID-19-mediated pneumonia. Our data support that 25-HC@DDAB can also downregulate inflammatory pathways. Furthermore, considering that cholesterol administration is a widely used strategy for the treatment of critically ill patients, the 25-HC@DDAB can be applied to the treatment of various respiratory infectious diseases.

Conclusion

In conclusion, we demonstrated inhibition of cytokine storm via downregulation of inflammatory NF-κB and SREBP2 signaling pathways in COVID-19 patient-derived PBMCs by using 25-HC@DDAB. The developed NHs could effectively accumulate lung tissues with remarkable accumulation efficiency. Moreover, 25-HC@DDAB in a septic mouse model exhibited enhancement of the survival rate. Considering the absence of approved therapeutics for SARS-CoV-2 pneumonia, it is anticipated that 25-HC@DDAB could be a promising candidate for modulation of lung tissue damage and cytokine storm in severe COVID-19 patients.

CRediT authorship contribution statement

Hyelim Kim: Formal analysis, Investigation, Methodology, Validation, Visualization. **Han Sol Lee:** Investigation, Methodology, Validation, Visualization. **June Hong Ahn:** Conceptualization, Data curation, Resources. **Kyung Soo Hong:** Data curation, Validation. **Jong Geol Jang:** Data curation, Validation. **Jiseon An:** Methodology. **Yong-Hyeon Mun:** Methodology. **So-Yeol Yoo:** Methodology. **Yoon Jung Choi:** Methodology. **Mi-Young Yun:** Methodology. **Gyu Yong Song:** Data curation, Validation. **Jinmyoung Joo:** Data curation, Validation. **Dong Hee Na:** Data curation, Funding acquisition, Validation. **Hong Nam Kim:** Conceptualization, Data curation, Formal analysis, Visualization, Funding acquisition, Roles/Writing - original draft. **Hee Ho Park:** Conceptualization, Data curation, Formal analysis, Funding acquisition, Visualization, Roles/Writing - original draft. **Jae-Young Lee:** Conceptualization, Data curation, Funding acquisition, Formal analysis, Roles/Writing - original draft;

Writing - review & editing. **Wonhwa Lee:** Conceptualization, Data curation, Project administration, Supervision, Validation, Visualization, Roles/Writing - original draft, Writing - review & editing.

Declaration of Competing Interest

The authors declare that they have no known competing financial interests or personal relationships that could have appeared to influence the work reported in this paper.

Acknowledgments

This work was supported by a grant from the National Research Foundation of Korea (NRF) funded by the Korean Government (MSIT) (Grant nos. 2018R1A2A3075013, 2021R1C1C1009320, 2018M3A7B4071204, 2018R1A2B3004266, 2020R1A4A3078645, 2021R1C1C1014606, 2021R1C1C2006896 and 2020R1A4A4079817).

Appendix A. Supplementary material

Supplementary data associated with this article can be found in the online version at doi:10.1016/j.nantod.2021.101149.

References

[1] T.T. Le, Z. Andreadakis, A. Kumar, R.G. Roman, S. Tollefsen, M. Saville, S. Mayhew, Evolution of the COVID-19 vaccine development landscape, Nat. Rev. Drug Discov. 19 (2020) 667–668.
[2] Y. Ge, T. Tian, S. Huang, F. Wan, J. Li, S. Li, H. Yang, L. Hong, N. Wu, E. Yuan, L. Cheng, Y. Lei, H. Shu, X. Feng, Z. Jiang, Y. Chi, X. Guo, L. Cui, L. Xiao, Z. Li, C. Yang, Z. Miao, H. Tang, L. Chen, H. Zeng, D. Zhao, F. Zhu, X. Shen, J. Zeng, bioRxiv (2020) 2020.2003.2011.986836.
[3] X. Cao, COVID-19: immunopathology and its implications for therapy, Nat. Rev. Immunol. 20 (2020) 269–270.
[4] M.Z. Tay, C.M. Poh, L. Rénia, P.A. MacAry, L.F. Ng, Nat. Rev. Immunol. (2020) 1–12.
[5] J. Hadjadj, N. Yatim, L. Barnabei, A. Corneau, J. Boussier, N. Smith, H. Pere, B. Charbit, V. Bondet, C. Chenevier-Gobeaux, P. Breillat, N. Carlier, R. Gauzit, C. Morbieu, F. Pene, N. Marin, N. Roche, T.A. Szwebel, S.H. Merkling, J.M. Treluyer, D. Veyer, L. Mouthon, C. Blanc, P.L. Tharaux, F. Rozenberg, A. Fischer, D. Duffy, F. Rieux-Laucat, S. Kerneis, B. Terrier, Impaired type I interferon activity and inflammatory responses in severe COVID-19 patients, Science 369 (2020) 718–724.
[6] J.G. McDonald, D.W. Russell, Editorial: 25-hydroxycholesterol: a new life in immunology, J. Leukoc. Biol. 88 (2010) 1071–1072.
[7] D.W. Russell, The enzymes, regulation, and genetics of bile acid synthesis, Annu. Rev. Biochem. 72 (2003) 137–174.
[8] H. Xiao, M. Lu, T.Y. Lin, Z. Chen, G. Chen, W.C. Wang, T. Marin, T.P. Shentu, L. Wen, B. Gongol, W. Sun, X. Liang, J. Chen, H.D. Huang, J.H. Pedra, D.A. Johnson, J.Y. Shyy, Sterol regulatory element binding protein 2 activation of NLRP3 inflammasome in endothelium mediates hemodynamic-induced atherosclerosis susceptibility, Circulation 128 (2013) 632–642.
[9] A. Reboldi, E.V. Dang, J.G. McDonald, G. Liang, D.W. Russell, J.G. Cyster, 25-Hydroxycholesterol suppresses interleukin-1–driven inflammation downstream of type I interferon, Science 345 (2014) 679–684.
[10] D.R. Jacobs Jr., B. Hebert, P.J. Schreiner, S. Sidney, C. Iribarren, S. Hulley, Reduced cholesterol is associated with recent minor illness The CARDIA study, Am. J. Epidemiol. 146 (1997) 558–564.
[11] W.R. Beisel, Cancer Res. 41 (1981) 3797–3798.
[12] W.R. Beisel, R.H. Fiser Jr., Lipid metabolism during infectious illness, Am. J. Clin. Nutr. 23 (1970) 1069–1079.
[13] C. Alvarez, A. Ramos, Lipids, lipoproteins, and apoproteins in serum during infection, Clin. Chem. 32 (1986) 142–145.
[14] R.S. Lees, R.H. Fiser Jr., W.R. Beisel, P.J. Bartelloni, Effects of an experimental viral infection on plasma lipid and lipoprotein metabolism, Metabolism 21 (1972) 825–833.
[15] K. Sammalkorpi, V. Valtonen, Y. Kerttula, E. Nikkila, M.R. Taskinen, Changes in serum lipoprotein pattern induced by acute infections, Metabolism 37 (1988) 859–865.
[16] W.H. Ettinger Jr., T. Harris, R.B. Verdery, R. Tracy, E. Kouba, Evidence for inflammation as a cause of hypocholesterolemia in older people, J. Am. Geriatr. Soc. 43 (1995) 264–266.
[17] H.W. Harris, C. Grunfeld, K.R. Feingold, J.H. Rapp, Human very low density lipoproteins and chylomicrons can protect against endotoxin-induced death in mice, J. Clin. Investig. 86 (1990) 696–702.
[18] H.W. Harris, C. Grunfeld, K.R. Feingold, T.E. Read, J.P. Kane, A.L. Jones, E.B. Eichbaum, G.F. Bland, J.H. Rapp, Chylomicrons alter the fate of endotoxin, decreasing tumor necrosis factor release and preventing death, J. Clin. Investig. 91 (1993) 1028–1034.
[19] Y. Zhang, Z. Song, M. Wang, M. Lan, K. Zhang, P. Jiang, Y. Li, J. Bai, X. Wang, Cholesterol 25-hydroxylase negatively regulates porcine intestinal coronavirus replication by the production of 25-hydroxycholesterol, Vet. Microbiol. 231 (2019) 129–138.
[20] J.T. Wu, K. Leung, M. Bushman, N. Kishore, R. Niehus, P.M. de Salazar, B.J. Cowling, M. Lipsitch, G.M. Leung, Estimating clinical severity of COVID-19 from the transmission dynamics in Wuhan, China, Nat. Med. 26 (2020) 506–510.
[21] G. Li, E. De Clercq, Therapeutic options for the 2019 novel coronavirus (2019-nCoV), Nat. Rev. Drug Discov. 19 (2020) 149–150.
[22] Q. Cheng, T. Wei, L. Farbiak, L.T. Johnson, S.A. Dilliard, D.J. Siegwart, Selective organ targeting (SORT) nanoparticles for tissue-specific mRNA delivery and CRISPR–Cas gene editing, Nat. Nanotechnol. 15 (2020) 313–320.
[23] Y. Hattori, A. Nakamura, S. Arai, K. Kawano, Y. Maitani, E. Yonemochi, siRNA delivery to lung-metastasized tumor by systemic injection with cationic liposomes, J. Liposome Res. 25 (2015) 279–286.
[24] K.-i Kusumoto, T. Ishikawa, Didodecyldimethylammonium bromide (DDAB) induces caspase-mediated apoptosis in human leukemia HL-60 cells, J. Control. Release 147 (2010) 246–252.
[25] P. Li, L. Zhang, K. Ai, D. Li, X. Liu, E. Wang, Coating didodecyldimethylammonium bromide onto Au nanoparticles increases the stability of its complex with DNA, J. Control. Release 129 (2008) 128–134.
[26] T. Skjørringe, T. Gjetting, T.G. Jensen, A modified protocol for efficient DNA encapsulation into pegylated immunoliposomes (PILs), J. Control. Release 139 (2009) 140–145.
[27] M. Singer, C.S. Deutschman, C.W. Seymour, M. Shankar-Hari, D. Annane, M. Bauer, R. Bellomo, G.R. Bernard, J.D. Chiche, C.M. Coopersmith, R.S. Hotchkiss, M.M. Levy, J.C. Marshall, G.S. Martin, S.M. Opal, G.D. Rubenfeld, T. van der Poll, J.L. Vincent, D.C. Angus, The third international consensus definitions for sepsis and septic shock (Sepsis-3), JAMA 315 (2016) 801–810.
[28] H.H. Park, H.N. Kim, H. Kim, Y. Yoo, H. Shin, E.Y. Choi, J.-S. Bae, W. Lee, 6, 2020, p. eabc1564.
[29] D. Rittirsch, M.S. Huber-Lang, M.A. Flierl, P.A. Ward, Immunodesign of experimental sepsis by cecal ligation and puncture, Nat. Protoc. 4 (2009) 31–36.
[30] F. Sun, G. Xiao, Z. Qu, In vitro assay to assess efficacy of potential antiviral compounds against enterovirus D68, Bio-Protocol 7 (2017).
[31] J. Xu, P. Zhou, W. Wang, A. Sun, F. Guo, RelB, together with RelA, sustains cell survival and confers proteasome inhibitor sensitivity of chronic lymphocytic leukemia cells from bone marrow, J. Mol. Med. 92 (2014) 77–92.
[32] C. Guo, Z. Chi, D. Jiang, T. Xu, W. Yu, Z. Wang, S. Chen, L. Zhang, Q. Liu, X. Guo, X. Zhang, W. Li, L. Lu, Y. Wu, B.L. Song, D. Wang, Cholesterol homeostatic regulator SCAP-SREBP2 integrates NLRP3 inflammasome activation and cholesterol biosynthetic signaling in macrophages, Immunity 49 (2018) 842–856.e7 e847.
[33] T. Greenhalgh, G.C.H. Koh, J. Car, Covid-19: a remote assessment in primary care, BMJ 368 (2020) m1182.
[34] C.J. Tignanelli, N.E. Ingraham, M.A. Sparks, R. Reilkoff, T. Bezdicek, B. Benson, T. Schacker, J.G. Chipman, M.A. Puskarich, Antihypertensive drugs and risk of COVID-19, Lancet Respir. Med. 8 (2020) e30–e31.
[35] M. Hoffmann, H. Kleine-Weber, S. Schroeder, N. Krüger, T. Herrler, S. Erichsen, T.S. Schiergens, G. Herrler, N.-H. Wu, A. Nitsche, Focus on causality in ESC/iPSC-based modeling of psychiatric disorders, Cells 9 (2020) 366-280.e8.
[36] K.C. Kao, L.C. Chiu, C.Y. Hung, C.H. Chang, C.T. Yang, C.C. Huang, H.C. Hu, Coinfection and mortality in pneumonia-related acute respiratory distress syndrome patients with bronchoalveolar lavage: a prospective observational study, Shock 47 (2017) 615–620.
[37] Q. Ye, B. Wang, J. Mao, The pathogenesis and treatment of the 'Cytokine Storm' in COVID-19, J. Infect. 80 (2020) 607–613.
[38] H. Wang, S. Ma, The cytokine storm and factors determining the sequence and severity of organ dysfunction in multiple organ dysfunction syndrome, Am. J. Emerg. Med. 26 (2008) 711–715.
[39] J. Hajj, N. Blaine, J. Salavaci, D. Jacoby, Healthcare 6 (2018) (Basel).
[40] G.L. Lin, J.P. McGinley, S.B. Drysdale, A.J. Pollard, Epidemiology and immune pathogenesis of viral sepsis, Front. Immunol. 9 (2018) 2147.
[41] W. Zhang, Y. Zhao, F. Zhang, Q. Wang, T. Li, Z. Liu, J. Wang, Y. Qin, X. Zhang, X. Yan, X. Zeng, S. Zhang, The use of anti-inflammatory drugs in the treatment of people with severe coronavirus disease 2019 (COVID-19): the perspectives of clinical immunologists from China, Clin. Immunol. 214 (2020) 108393.
[42] V. Pooladanda, S. Thatikonda, C. Godugu, The current understanding and potential therapeutic options to combat COVID-19, Life Sci. 254 (2020) 117765.
[43] Q. Liu, Y.-h. Zhou, Z.-q. Yang, The cytokine storm of severe influenza and development of immunomodulatory therapy, Cell. Mol. Immunol. 13 (2016) 3–10.
[44] H. Xiao, M. Lu, T.Y. Lin, Z. Chen, G. Chen, W.-C. Wang, T. Marin, T.-p. Shentu, L. Wen, B. Gongol, Sterol regulatory element binding protein 2 activation of NLRP3 inflammasome in endothelium mediates hemodynamic-induced atherosclerosis susceptibility, Circulation 128 (2013) 632–642.
[45] S. Zu, Y.-Q. Deng, C. Zhou, J. Li, L. Li, Q. Chen, X.-F. Li, H. Zhao, S. Gold, J. He, 25-Hydroxycholesterol is a potent SARS-CoV-2 inhibitor, Cell Res. 30 (2020) 1043–1045.
[46] R. Zang, J.B. Case, E. Yutuc, X. Ma, S. Shen, M.F.G. Castro, Z. Liu, Q. Zeng, H. Zhao, J. Son, Cholesterol 25-hydroxylase suppresses SARS-CoV-2 replication by blocking membrane fusion, Proc. Natl. Acad. Sci. USA 117 (2020) 32105–32113.